Uniform approach to linear and nonlinear interrelation patterns in multivariate time series

Christian Rummel,[1,2,*] Eugenio Abela,[1,3] Markus Müller,[4,5] Martinus Hauf,[1] Olivier Scheidegger,[1] Roland Wiest,[1] and Kaspar Schindler[2]

[1]*Support Center for Advanced Neuroimaging (SCAN), Institute of Diagnostic and Interventional Neuroradiology, Inselspital, Bern University Hospital, University of Bern, CH-3010 Bern, Switzerland*

[2]*qEEG group, Department of Neurology, Inselspital, Bern University Hospital, University of Bern, CH-3010 Bern, Switzerland*

[3]*Department of Neurology, Kantonsspital St. Gallen, CH-9007 St. Gallen, Switzerland*

[4]*Facultad de Ciencias, Universidad Autónoma del Estado de Morelos, Morelos C. P. 62209, Cuernavaca, Mexico*

[5]*Centro Internacional de Ciencias AC, Universidad Nacional Autónoma de México, Morelos C. P. 62209, Cuernavaca, Mexico*

(Received 22 December 2010; revised manuscript received 8 April 2011; published 30 June 2011)

Currently, a variety of linear and nonlinear measures is in use to investigate spatiotemporal interrelation patterns of multivariate time series. Whereas the former are by definition insensitive to nonlinear effects, the latter detect both nonlinear and linear interrelation. In the present contribution we employ a uniform surrogate-based approach, which is capable of disentangling interrelations that significantly exceed random effects and interrelations that significantly exceed linear correlation. The bivariate version of the proposed framework is explored using a simple model allowing for separate tuning of coupling and nonlinearity of interrelation. To demonstrate applicability of the approach to multivariate real-world time series we investigate resting state functional magnetic resonance imaging (rsfMRI) data of two healthy subjects as well as intracranial electroencephalograms (iEEG) of two epilepsy patients with focal onset seizures. The main findings are that for our rsfMRI data interrelations can be described by linear cross-correlation. Rejection of the null hypothesis of linear iEEG interrelation occurs predominantly for epileptogenic tissue as well as during epileptic seizures.

DOI: 10.1103/PhysRevE.83.066215 PACS number(s): 05.45.Tp, 02.50.Sk, 87.19.L−, 89.75.Fb

I. INTRODUCTION

Physiologic time series are often multivariate in the sense that various channels are recorded, which either represent different types of data (e.g., heart rate, blood pressure, breath rate, and oxygen saturation) or the same type of data recorded from different spatial locations (e.g., multichannel electrocardiogram or electroencephalogram). Quantitative analysis of this type of time series can be divided into three disciplines, concentrating on univariate or bi- and multivariate aspects. Whereas the univariate approaches treat data channels as if they were completely independent of each other, the purpose of bi- and multivariate approaches is investigation of *interrelations* between channel pairs or even within the whole system.

Two time series $X_1(t)$ and $X_2(t)$ are interrelated if knowledge of $X_1(t)$ confines the range of $X_2(t)$ (or vice versa). In scatter plots of X_2 against X_1 interrelation becomes visible by cumulation of the data. If the interrelation is *linear*, i.e.,

$$X_2(t) = a + bX_1(t) + \epsilon(t) \tag{1}$$

with some error $\epsilon(t)$, the cumulation is around a straight line with intercept a and slope b. Its amount can be quantified by Pearson's product-moment correlation coefficient. More generally, interrelation can be described by a mapping

$$X_2(t) = f[X_1(t)] + \epsilon(t) \tag{2}$$

with some function $f[\cdot]$. In many cases a *linear approximation* to $f[\cdot]$ may describe the character of the interrelation considerably well. However, if interrelation is significantly stronger than described by Eq. (1) we term it *significantly nonlinear*.

A nonlinear time-series analysis of neurophysiologic data [1–3] has long been "en vogue." Later, the importance of nonlinearity in neurophysiological time series, and especially the capability of measures to detect these reliably from short and noisy experimental data, has been challenged. As a univariate example, signs of low dimensional chaos as measured by the correlation dimension of electroencephalographic (EEG) data turned out to be insignificant after careful re-examination of the data by the same authors [4,5]. Comparing the sensitivity and specificity of various bivariate interrelation measures for model data, it was recently found that linear measures perform equally well or even better than nonlinear measures—even if the signals or the interrelation were indeed nonlinear [6–8]. Finally, in the context of epileptic seizure prediction using intracranial electroencephalographic (iEEG) data it has been shown that linear cross-correlation may outperform sophisticated nonlinear measures in terms of sensitivity and specificity [9,10].

Focusing on bivariate and multivariate analysis strategies, the present paper tries to contribute to the debate between supporters of nonlinear and linear approaches. Using a rigorous hypothesis testing paradigm based on uni- and multivariate linear surrogates and cross-correlation and mutual information as interrelation measures, we separate for each channel pair, (i) linear correlation that goes significantly beyond what is possible for completely independent signals with conserved univariate linear properties ("significant linear correlation") and (ii) mutual information that goes significantly beyond the degree explained by linear time series with the same

*crummel@web.de; Corresponding author: Christian Rummel, SCAN, Institute of Diagnostic and Interventional Neuroradiology, Inselspital, Bern University Hospital, University of Bern, CH-3010 Bern, Switzerland.

cross-correlation pattern (despite caveats [11] we occasionally denote this type as "significantly nonlinear interrelation" here).

Whereas the general idea for this type of hypothesis testing already has been applied to pairs of time series [3,11] (for recent applications, see Refs. [12–15]), we here propose a computationally feasible variant that qualifies for data of high dimensionality and time-resolved applications. In addition, we investigate the implications of rejection of our null hypotheses on truly multivariate entities like eigenvalues and eigenvectors of interrelation matrices. In this way we assess the system character of the multivariate time series, which has the potential to reveal different information than an approach limited to bivariate aspects.

The paper is organized as follows: In Sec. II we discuss equal-time cross-correlation and mutual information. As an extension of the concept of the cross-correlation–based matrix $\mathcal{M}_{ij}^{\mathrm{CCS}}$ introduced in Ref. [16] to mutual information, novel bivariate measures are suggested, which concentrate on special aspects of the interrelation. The performance of these is tested at the example of a simple tunable model in Sec. III. Thereafter, application to neurophysiological data [resting state functional magnetic resonance imaging (rsfMRI) and periseizure iEEG] is made in Sec. IV. Finally, results are summarized and discussed in Sec. V.

II. LINEAR AND NONLINEAR INTERRELATION MEASURES

A. Cross-correlation and mutual information

A common interrelation measure is given by Pearson's equal-time (zero-lag) cross-correlation (CC)

$$C_{ij} = \frac{1}{T}\sum_{t=1}^{T} \tilde{X}_i(t)\tilde{X}_j(t) \in [-1,1], \tag{3}$$

where the tilde denotes normalization of the time series $X_i(t)$ to zero mean and unit variance ($i = 1,\ldots,M$ counts the channels of the multivariate data set and $t = 1,\ldots,T$ is the temporal sample point, given a piece of length T). Equation (3) allows computationally effective and robust estimation of dependencies even between short and noise-corrupted time series. Despite these favorable features there is the drawback of being limited to linear interrelation *a priori*, i.e., missing even simple nonlinear relations. The most prominent example where CC fails completely to report interrelation is $X_2(t) = (X_1(t))^2$.

A generalization of Eq. (3) based on information theory that is applicable independently from any model assumption and especially not restricted to Gaussianity or linear interrelation is given by mutual information (MI)

$$I_{ij} = \sum_{i,j} p_{ij} \log \frac{p_{ij}}{p_i p_j} \geqslant 0. \tag{4}$$

It quantifies the deviation of the joint distribution p_{ij} of the signal amplitudes $X_i(t)$ and $X_j(t)$ from the product $p_i p_j$ of the marginal distributions $p_i = \sum_j p_{ij}$ and $p_j = \sum_i p_{ij}$, which implies statistical independence and $I_{ij} = 0$. For correlated Gaussian noise there is a one-to-one correspondence between MI and CC:

$$I_{ij} \geqslant I_{ij}^{\mathrm{G}} = -\frac{1}{2}\log\left(1 - C_{ij}^2\right). \tag{5}$$

The inequality can be used to find a lower bound for MI and quantify the deviation of the data from Gaussianity [14]. Inspired by the relation of Eq. (5) we normalize MI to the interval [0,1] using the transformation [17]

$$\mathrm{NMI}_{ij} = \sqrt{1 - \exp(-2I_{ij})} \in [0,1], \tag{6}$$

which warrants $\mathrm{NMI}_{ij}^{\mathrm{G}} = |C_{ij}|$ for Gaussian data.

In the present study, MI is estimated from time series using the k-nearest-neighbor algorithm [18] as implemented in the publicly available MILCA package (http://www.klab.caltech.edu/~kraskov/MILCA/). In a recent comparative study this algorithm has been shown to be superior to other estimators, especially for short ($T \lesssim 1000$) and noisy time series [19]. We use the same value $k = 3$ as in the comparative study. This choice of a small k reduces the bias of the estimator at the expense of larger variance [18]. In addition, the computational workload is smaller for small k.

B. Specialized interrelation measures

In Refs. [16,20] CC-based interrelation measures were introduced that focus on complementary aspects of equal-time cross-correlation. Surrogate data were employed to test the null hypothesis of purely random correlation between independent time series of length T and given power spectrum. Separate matrices sensitive to "random correlations" and "genuine cross-correlations" were defined.

Here, we generalize the previously introduced procedure in two directions. First, we use two types of interrelation measures: CC of Eq. (3) and NMI of Eq. (6). If not further specified, normalized bivariate interrelation measures are denoted by the placeholder A_{ij} in the sequel ($-1 \leqslant A_{ij} \leqslant 1$ and $A_{ii} = 1$). Second, we test two types of null hypotheses that the observed multivariate time series is produced by

H_0^{uni}: two *independent univariate* stochastic linear processes fulfilling the requirements of stationarity and Gaussianity or

H_0^{multi}: one *multivariate* stochastic linear process with given linear cross-correlation patterns and fulfilling the requirements of stationarity and Gaussianity.

In both cases the observations might have been distorted by monotonic but nonlinear measurement functions. For testing these null hypotheses, iterative amplitude adjusted Fourier transform (IAAFT) surrogate data are used. If not specified further, the surrogates will be denoted by the placeholder B in the sequel. Under randomization *independent univariate* IAAFT surrogates [21] destroy all nonlinear features of the input time series as well as correlations between them but conserve linear univariate properties (amplitude distributions, autocorrelations, power spectra). In addition *multivariate* IAAFT surrogates [22] also conserve the linear cross-correlations between the input signals under randomization. These features make univariate and multivariate IAAFT surrogates ideal frameworks to test H_0^{uni} and H_0^{multi}, respectively.

TABLE I. Nomenclature for specialized interrelation measures $\mathcal{M}_{ij}^{A,B}$.

Measure	Interrelation measure A	Null hypothesis N	Surrogates B
$\mathcal{M}_{ij}^{\mathrm{CC,uni}}$	CC	H_0^{uni}	Univariate IAAFT
$\mathcal{M}_{ij}^{\mathrm{CC,multi}}$	CC	H_0^{multi}	Multivariate IAAFT
$\mathcal{M}_{ij}^{\mathrm{NMI,uni}}$	NMI	H_0^{uni}	Univariate IAAFT
$\mathcal{M}_{ij}^{\mathrm{NMI,multi}}$	NMI	H_0^{multi}	Multivariate IAAFT

Although, in general, all conceivable inversions of the formulations of H_0^{uni} and H_0^{multi} can lead to rejections of the null hypotheses, see, e.g., the discussion in Ref. [11], we interpret rejection of H_0^{uni} in the sense that observed interrelations are likely beyond random effects. Similarly we interpret rejection of H_0^{multi} as a strong sign for nonlinearity in the interrelations. Construction of surrogates that explicitly exclude all conceivable alternative causes for rejection of H_0^{multi} (e.g., nonstationary or non-Gaussian stochastic processes) except nonlinearity of the interrelation is a very hard task, if not impossible.

In the following we integrate interrelation measures A and surrogate data B into a uniform framework of four bivariate measures $\mathcal{M}_{ij}^{A,B}$ that quantify different aspects of the dynamics and allow us to disentangle linear from nonlinear interrelations; see Table I. Depending on the testable null hypothesis, for the input time series a set of N_{surr} surrogate time series $X_i^B(t)$ of type B is generated from a portion of data of length L first. Surrogate and original time series are then subdivided into N_{ens} possibly overlapping segments of length $T < L$ and the interrelation measure A_{ij} is calculated for each segment. As a result, one obtains samples of N_{ens} interrelation estimates $A_{ij}^{(n)}$ between the original time-series segments $X_i^{(n)}(t)$ and $X_j^{(n)}(t)$ $(n = 1, \ldots, N_{\mathrm{ens}})$ as well as $N_{\mathrm{surr}}N_{\mathrm{ens}}$ estimates $A_{ij}^{B,(n,n')}$ for the surrogate segments $X_i^{B,(n,n')}(t)$ and $X_j^{B,(n,n')}(t)$ ($n = 1, \ldots, N_{\mathrm{ens}}$ and $n' = 1, \ldots, N_{\mathrm{surr}}$). To fix the notation we define the medians $\mu_{ij} = \mathrm{med}\{|A_{ij}^{(n)}|\}$, $\mu_{ij}^B = \mathrm{med}\{|A_{ij}^{B,(n,n')}|\}$, $\nu_{ij} = \mathrm{med}\{A_{ij}^{(n)}\}$, and $\nu_{ij}^B = \mathrm{med}\{A_{ij}^{B,(n,n')}\}$ of the absolute and signed interrelation coefficients of the ensembles of original and surrogate time series, respectively. Following [16] we define

$$\mathcal{M}_{ij}^{A,B} = \mathrm{sign}(\nu_{ij})\frac{\mu_{ij} - \mu_{ij}^B}{1 - \mu_{ij}^B} s_{ij} \quad \text{for } i \neq j \tag{7}$$

and $\mathcal{M}_{ii}^{A,B} \equiv 1$. In Eq. (7) the numerator quantifies the amount of interrelation between signals X_i and X_j that cannot be explained by the surrogates B and s_{ij} indicates the significance of the difference. Note that it is the median of the absolute interrelation coefficients μ_{ij} that enters Eq. (7). The denominator puts all channel pairs i and j on the same scale independently and assures that for identical time series $\mathcal{M}_{ij}^{A,B} = 1$. As the distribution of the absolute matrix elements $|A_{ij}|$ and $|A_{ij}^B|$ cannot be expected to be Gaussian (their distribution is confined to the interval [0,1] and very skew) we use a nonparametric test procedure for determination of s_{ij}. The difference $\mu_{ij} - \mu_{ij}^B$ is accepted on a significance level $0 < \alpha' < 1$ only if a Mann-Whitney-Wilcoxon U test [23] rejects the null hypothesis of equal medians. In this case we let $s_{ij} = 1$ and $s_{ij} = 0$ otherwise.

Due to possible spatial and temporal dependencies, exact determination of the significance is a hard task. Here we resort to approximation. In order to have an overall chance $0 < \alpha < 1$ of an M-dimensional matrix $\mathcal{M}_{ij}^{A,B}$ with one or several elements that were erroneously judged significant the significance level α is Bonferroni corrected for multiple U tests $\alpha \to \alpha' = 2\alpha/[M(M-1)]$. Thus, in the multivariate situation the testing procedure implies that the matrices $\mathcal{M}_{ij}^{A,B}$ occasionally become very sparse, i.e., they have many off-diagonal elements, $\mathcal{M}_{ij}^{A,B} = 0$.

The calculation of Eq. (7) involves several parameters, some of which can be confined by physical properties of the time series under investigation. The segments L used for surrogate generation have to be long enough to contain several cycles of the lowest frequencies present in the data and short enough to account for possible nonstationarities. In addition to $T < L$ in the multivariate case we have to demand $T > M$ to avoid spurious rank deficiency of the interrelation matrices A_{ij} due to dependence of its elements.

Large ensemble sizes N_{ens} and N_{surr} are desirable as they make the U tests more powerful. However, $N_{\mathrm{ens}} > \lfloor L/T \rfloor$ leads to overlapping segments and, consequently, to potential serial dependence of ensemble members A_{ij}, which may bias the outcome of the U test used to fix s_{ij} in Eq. (7). Last but not least, the computational workload needed to estimate the matrices $\mathcal{M}_{ij}^{A,B}$ is proportional to the number of surrogates N_{surr}. In Sec. III B we investigate the dependence of the interrelation estimates of Eq. (7) on N_{ens} and N_{surr}.

Equation (7) is a generalization of the matrix $\mathcal{M}_{ij}^{\mathrm{CCS}}$ introduced in Ref. [16], which represents the special case where $A_{ij} = C_{ij}$ and B are univariate IAAFT surrogates. The matrix $\mathcal{M}_{ij}^{\mathrm{CC,uni}} \equiv \mathcal{M}_{ij}^{\mathrm{CCS}}$ (see Table I) identifies genuine cross-correlations beyond the randomly present correlation in independent time series of equal length and power spectrum. Without using the normalized form of Eq. (7) a similar bootstrapping approach to significance of (maximal finite-lag) cross-correlation has independently been undertaken in Ref. [12]. Note that, by construction, $\mathcal{M}_{ij}^{\mathrm{CC,multi}}$ (see Table I) is expected to resemble the identity matrix.

III. BIVARIATE APPLICATION TO MODEL DATA

Before application of the definition Eq. (7) to multivariate neurophysiological time series in Sec. IV we investigate its performance using the example of a simple bivariate model with tunable coupling and nonlinearity.

A. The model

As a test frame that combines realistic univariate features of arbitrary real-world input time series with tunable coupling and nonlinearity we use a mixing model similar to the one suggested in Ref. [24] to produce a pair $X_1(t)$ and $X_2(t)$ of interrelated time series of length L. From the type of real-world signals one wants to simulate, four independent univariate IAAFT surrogate signals are generated: $\xi_1(t)$, $\xi_2(t)$, $\alpha(t)$, and

$\beta(t)$. Rather than applying them for hypothesis testing we here solely exploit that in univariate IAAFT surrogates by construction all nonlinearities and cross-correlation between the input signals are destroyed. The surrogates as well as the squared time series $\beta^2(t)$ are normalized separately to zero mean and unit variance. The procedure of signal normalization is denoted by a tilde here; see Eqs. (8) to (11).

Two coupling time series $\zeta_1(t)$ and $\zeta_2(t)$ are defined by

$$\zeta_1(t) = \frac{1}{\mathcal{N}_\zeta}[(1-\sigma)\widetilde{\alpha(t)} + \sigma\widetilde{\beta(t)}] \tag{8}$$

$$\zeta_2(t) = \frac{1}{\mathcal{N}_\zeta}[(1-\sigma)\widetilde{\alpha(t)} + \sigma\widetilde{\beta^2(t)}] \tag{9}$$

and mixed with independent components $\xi_1(t)$ and $\xi_2(t)$ with coupling strength ρ:

$$X_1(t) = \frac{1}{\mathcal{N}_X}[(1-|\rho|)\widetilde{\xi_1(t)} + |\rho|\zeta_1(t)] \tag{10}$$

$$X_2(t) = \frac{1}{\mathcal{N}_X}[(1-|\rho|)\widetilde{\xi_2(t)} + \rho\zeta_2(t)] \tag{11}$$

With $0 \leqslant \sigma \leqslant 1$ and $-1 \leqslant \rho \leqslant 1$ and using the normalization constants

$$\mathcal{N}_\zeta = 1 - 2\sigma + 2\sigma^2 \tag{12}$$

$$\mathcal{N}_X = 1 - 2|\rho| + 2\rho^2 \tag{13}$$

the signals $\zeta_1(t)$, $\zeta_2(t)$, $X_1(t)$, and $X_2(t)$ are automatically normalized. The *nonlinearity parameter* σ of Eqs. (8) and (9) switches between entirely linear ($\sigma = 0$) and quadratic ($\sigma = 1$) interrelation and the *mixing parameter* ρ of Eqs. (10) and (11) controls sign and degree of interrelation between $X_1(t)$ and $X_2(t)$. Note that, due to the employment of surrogates of real-world input signals, the output time series $X_1(t)$ and $X_2(t)$ still mimic their univariate linear properties [24] (see Fig. 1 of that publication).

B. Performance

The model of Eqs. (8)–(13) was used to investigate the performance of the interrelation measures $\mathcal{M}_{ij}^{A,B}$ for varying coupling ρ and nonlinearity σ. Simulations ($N = 20$) of the model were performed starting from the same bivariate real-world time series as input but different realizations of IAAFT surrogates for $\xi_1(t), \xi_2(t), \alpha(t)$, and $\beta(t)$. For each cycle the whole ρ-σ-parameter space was scanned. Figures 1 and 2 show the resulting interrelation estimates for the model using surrogates of rsfMRI time series as input. Segments overlapped 86%. Without showing additional figures we note that we found qualitatively the same behavior for surrogates of rsfMRI time series with half and double T as well as for surrogates of nonseizure and seizure iEEG time series with $f_{\text{samp}} = 512$ Hz, $L = 512, 1024, 2048, 4096$, and $T = L/2$. The similarity of our simulation results for iEEG signals recorded from so drastically different conditions over a wide range of L and T provides confidence that the influence of the potentially confounding factor nonstationarity on our interpretation of $\mathcal{M}_{ij}^{A,B}$ is not too large. Using surrogates of rsfMRI data as input we also checked that the MI-based measures are almost insensitive to the choice of k in the wide range $k = 3, \ldots, 11$.

Figures 1(a) and 1(b) reveal that linear CC decreases with increasing nonlinearity σ. The reason is that a linear approximation to the nonlinear interrelation becomes inappropriate when σ becomes too large. The measure $\mathcal{M}_{1,2}^{\text{CC,uni}} \equiv \mathcal{M}_{1,2}^{\text{CCS}}$ originally introduced in Ref. [16] and displayed in Figures 1(c) and 1(d) reveals that for $\sigma \gtrsim 0.5$ the linear correlation detected by CC is no longer significant. The same is true for $|\rho| \lesssim 0.5$, where coupling is too small to induce significant interrelation. Finally, utilizing CC as interrelation measure and normalizing to multivariate surrogates as done in $\mathcal{M}_{1,2}^{\text{CC,multi}}$, no significant deviation of cross-correlation between the original data and the surrogates can be detected anywhere in the ρ-σ plane [Figs. 1(e) and 1(f)]. This result confirms the theoretical

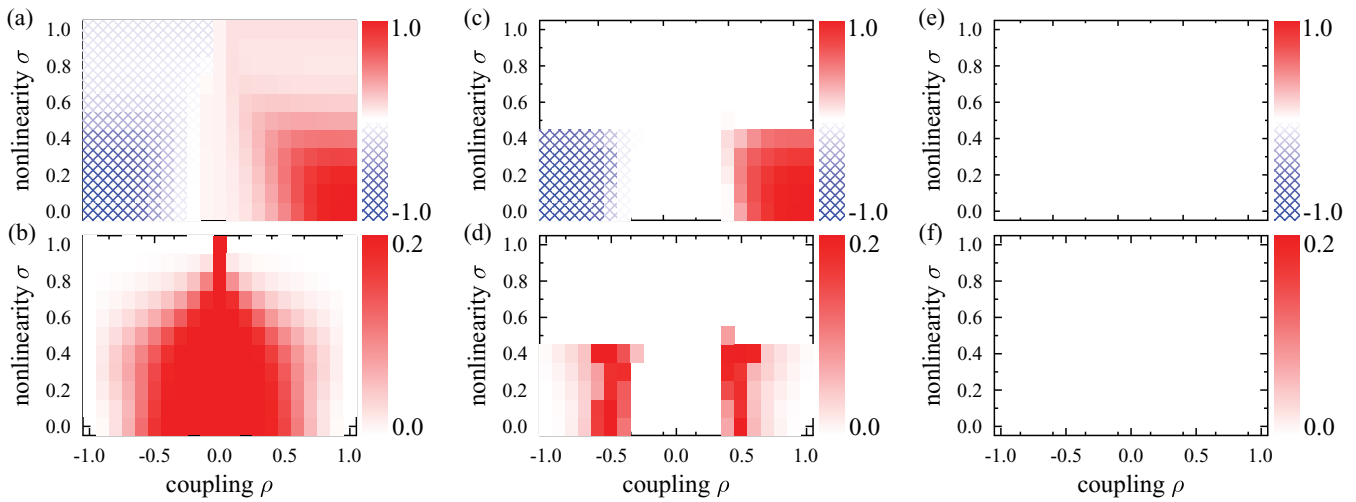

FIG. 1. (Color online) Interrelation estimates for cross-correlation–based measures. The test framework of Eqs. (8)–(13) was based on real-world rsfMRI time series with $f_{\text{samp}} = 0.5$ Hz, $L = 256$, and $T = 128$. $N_{\text{surr}} = 10$ IAAFT surrogates were produced and ensemble size was $N_{\text{ens}} = 8$. The significance level for U tests was set to $\alpha = 0.01$. [(a) and (b)] Equal-time cross-correlation $C_{1,2}$; [(c) and (d)] $\mathcal{M}_{1,2}^{\text{CC,uni}}$; and [(e) and (f)] $\mathcal{M}_{1,2}^{\text{CC,multi}}$. The top and bottom panels show average and standard deviation of the estimates over $N = 20$ independent realizations, respectively. Note that the color scale differs in the top and bottom panels.

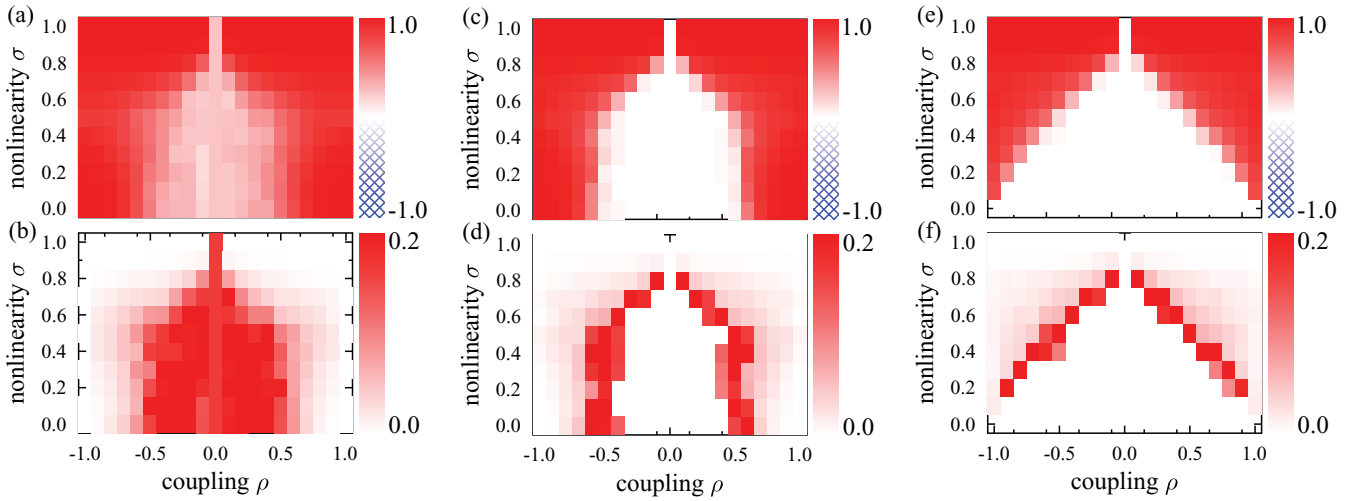

FIG. 2. (Color online) Mutual information-based interrelation estimates ($k = 3$) for the same data Fig. 1: [(a) and (b)] normalized mutual information $\mathrm{NMI}_{1,2}$; [(c) and (d)] $\mathcal{M}_{1,2}^{\mathrm{NMI,uni}}$; [(e) and (f)] $\mathcal{M}_{1,2}^{\mathrm{NMI,multi}}$.

expectation and shows that the measures are well defined and numerical errors of our implementation are small.

Using the same data and normalized MI as underlying interrelation measure the results are displayed in Fig. 2 . NMI is sensitive to linear as well as nonlinear coupling but cannot distinguish the sign of ρ [Figs. 2(a) and 2(b)]. The measure $\mathcal{M}_{1,2}^{\mathrm{NMI,uni}}$ shown in Figs. 2(c) and 2(d) is finite only if the null hypothesis H_0^{uni} is rejected; see the definition of s_{ij} in Eq. (7). Our simulation demonstrates that even weak coupling (small $|\rho|$) is revealed with significance if the nonlinearity is large enough ($\sigma \gtrsim 0.8$). Note that in Fig. 1(c) linear correlation

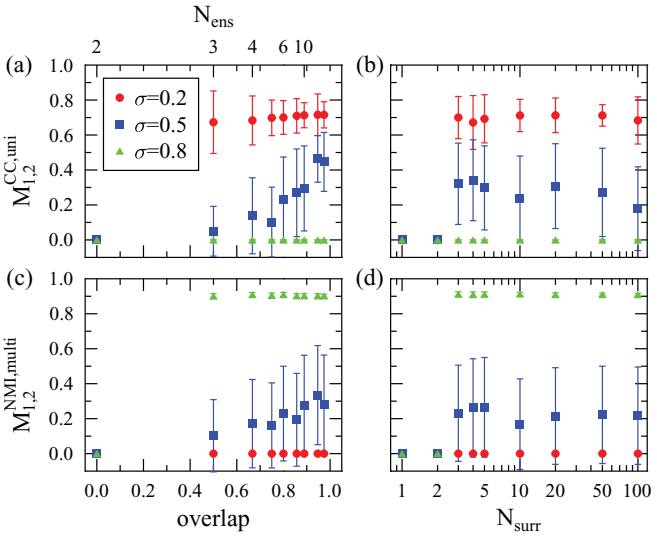

FIG. 3. (Color online) Dependence of the interrelation estimates $\mathcal{M}_{1,2}^{\mathrm{CC,uni}}$ (top) and $\mathcal{M}_{1,2}^{\mathrm{NMI,multi}}$ (bottom) on the ensemble size parameters. Results are shown for rsfMRI time series as input data for the model of Eqs. (8)–(13). In the left panels $N_{\mathrm{surr}} = 10$ is fixed, whereas N_{ens} is varied, determining the overlap of segments of length $T = 128$ within $L = 256$. On the right $N_{\mathrm{ens}} = 8$ is fixed, while the number of surrogates N_{surr} varies. The coupling is chosen as $\rho = 0.6$ in all panels and three degrees of nonlinearity σ are tested. Mean and standard deviation are estimated from $N = 100$ independent runs.

turned out to be insignificant in this region of the parameter space.

In Figs. 2(e) and 2(f) the performance of the newly introduced measure $\mathcal{M}_{1,2}^{\mathrm{NMI,multi}}$ is demonstrated. Values are more significant for larger nonlinearity σ and coupling $|\rho|$. As expected, for weakly coupled, weakly nonlinear situations the null hypothesis H_0^{multi} cannot not be rejected. For increasing nonlinearity $\sigma > 0$ the coupling strength $|\rho|$ needed for rejection decreases linearly, confirming that $\mathcal{M}_{1,2}^{\mathrm{NMI,multi}}$ may be utilized to detect significantly nonlinear coupling, i.e., situations where a linear approximation becomes insufficient.

Based on these findings we recommend a combined use of the matrices $\mathcal{M}_{1,2}^{\mathrm{CC,uni}}$ [Figs. 1(c) and 1(d)] and $\mathcal{M}_{1,2}^{\mathrm{NMI,multi}}$ [Fig. 2(e) and 2(f)] to disentangle purely linear and nonlinear features. The first measure is blind to nonlinear effects but detects genuine (i.e., nonspurious, nonrandom) linear cross-correlation, whereas the second is sensitive to interrelation that cannot be explained by linear interrelation.

We tested the dependence of our interrelation estimates on the choice of N_{ens} and N_{surr}. In Fig. 3 coupling was chosen as $\rho = 0.6$ and nonlinearity σ was varied. From Figs. 1(b) and 1(d) it becomes clear that, except for very small $N_{\mathrm{surr}} \leqslant 2$, the means and standard deviations of $\mathcal{M}_{1,2}^{\mathrm{CC,uni}}$ and $\mathcal{M}_{1,2}^{\mathrm{NMI,multi}}$ are independent of the number of surrogates. This remarkable behavior allows us to keep N_{surr} (and computation time) small. The reason can be traced back to the use of nonparametric statistics, as both the medians μ and the U tests entering Eq. (7) are known to be very robust. The uncertainties of the estimates are largest for $\sigma = 0.5$, where $\mathcal{M}_{1,2}^{\mathrm{CC,uni}}$ loses and $\mathcal{M}_{1,2}^{\mathrm{NMI,multi}}$ gains sensitivity, cf. Figs. 1(c), 1(d), 2(e), and 2(f). We have checked that for larger ρ these uncertainties become smaller. Also the dependence on N_{ens} [Figs. 1(a) and 1(c)] is small, except for those parameter regions where $\mathcal{M}_{1,2}^{\mathrm{CC,uni}}$ and $\mathcal{M}_{1,2}^{\mathrm{NMI,multi}}$ have large fluctuations; see Figs. 1(d) and 2(f). The deviating estimates at $N_{\mathrm{surr}} = 1,2$ (very small surrogate ensembles) and $N_{\mathrm{ens}} = 2$ (zero overlap of segments) can be explained from the fact that for these choices the ensembles are

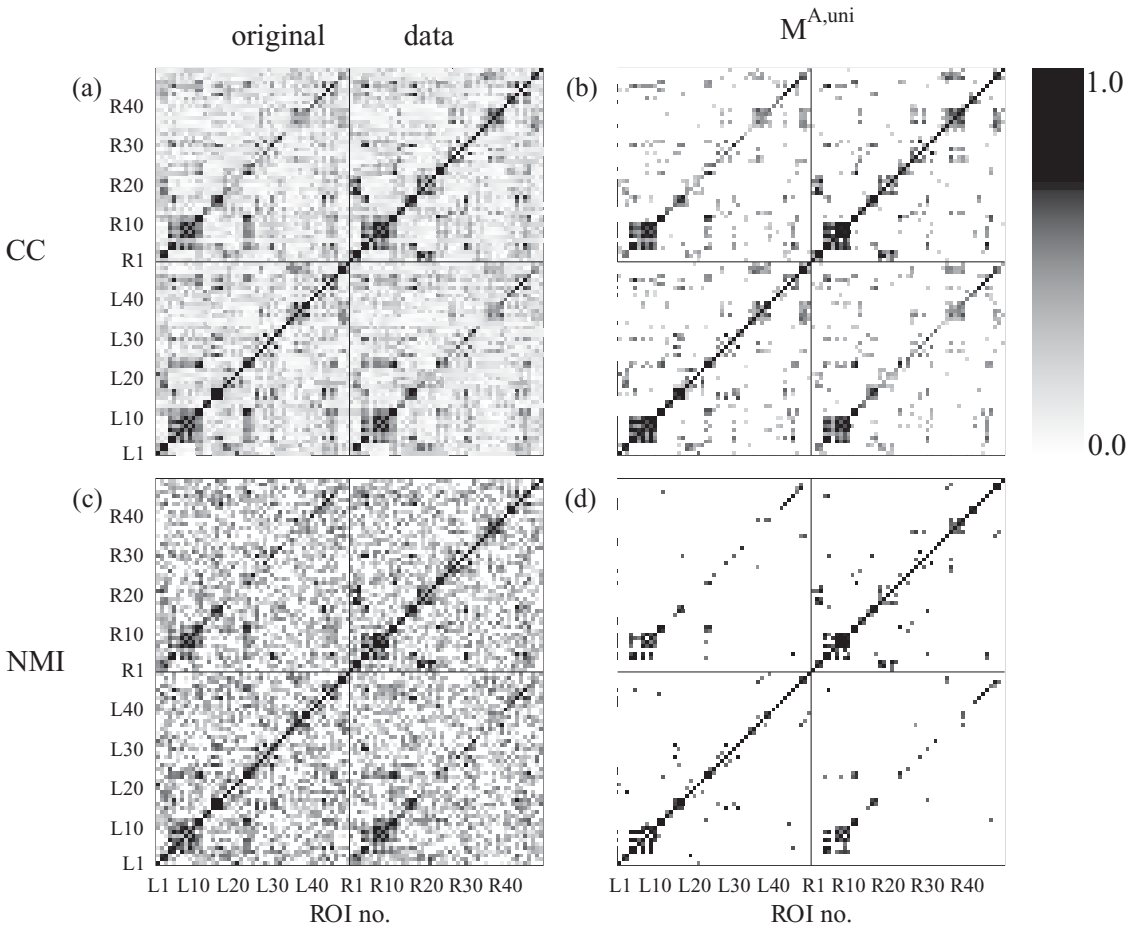

FIG. 4. Absolute values of interrelation matrices for ROI time series of a rsfMRI measurement of subject 1. Channels L1–L49 correspond to the left hemisphere and channels R1–R49 to the right hemisphere.

too small and consequently the U tests lack discrimination power.

IV. MULTIVARIATE APPLICATION TO NEUROPHYSIOLOGICAL TIME SERIES

Having explored the performance of the interrelation measures $\mathcal{M}_{ij}^{A,B}$ using bivariate model time series we now proceed to applying the measures to two types of multivariate neurophysiological time series. The EEG directly measures the integrated electrical activity of millions of neurons with excellent temporal (millisecond range) but limited spatial resolution (several square centimeters for scalp EEG). In certain epilepsy patients it can become necessary to improve the small spatial resolution and reduce sizable artifact corruption of scalp EEG by implanting intracranial electrodes. Intracranial EEG has better signal-to-noise ratio and spatial resolution (square millimeter range); however, this is at the expense of reduced spatial sampling due to incomplete coverage of the cortex. The limitations of EEG are contrasted by functional magnetic resonance imaging (fMRI), which measures the metabolic response to electrical brain activity via the blood oxygen level–dependent (BOLD) contrast. fMRI has excellent spatial sampling and resolution [volumetric image elements ("voxels") of only a few cubic millimeters] but limited temporal resolution (range of seconds).

A. Resting-state functional magnetic resonance imaging of healthy volunteers

First, we applied our method to investigate functional connectivity (FC) of the human brain using BOLD-fMRI. Functional connectivity has been defined as the temporal correlation of spatially distant neuropyhsiological time series [25] and thus is a good choice to test our analysis framework. Strong FC between brain regions has been recently found in synchronous, low-frequency BOLD-signal fluctuations of awake subjects lying in the MR scanner without performing experimental tasks ("resting-state FC," rsFC); see Ref. [26] for a review. Patterns of resting-state FC show a high degree of topographical symmetry between brain hemispheres and are highly reproducible within and between subjects; see, e.g., Refs. [27,28]. One of the most common approaches to rsFC consists in defining a set of regions of interest (ROI) across the brain, based on neuroanatomical criteria or prior experimental hypotheses, and compute the CC of their bandpass filtered BOLD-signal time series, e.g., Refs. [27,29].

For the MRI data acquisition of two healthy male volunteers (age 32 and 36 years), we used a 3-T Siemens Magnetom Trio TIM MR Scanner (Erlangen, Germany). Resting-state fMRI data were acquired using a multislice single-shot T2* -weighted echo planar imaging (EPI) sequence with 35 slices. Three hundred functional volumes were measured

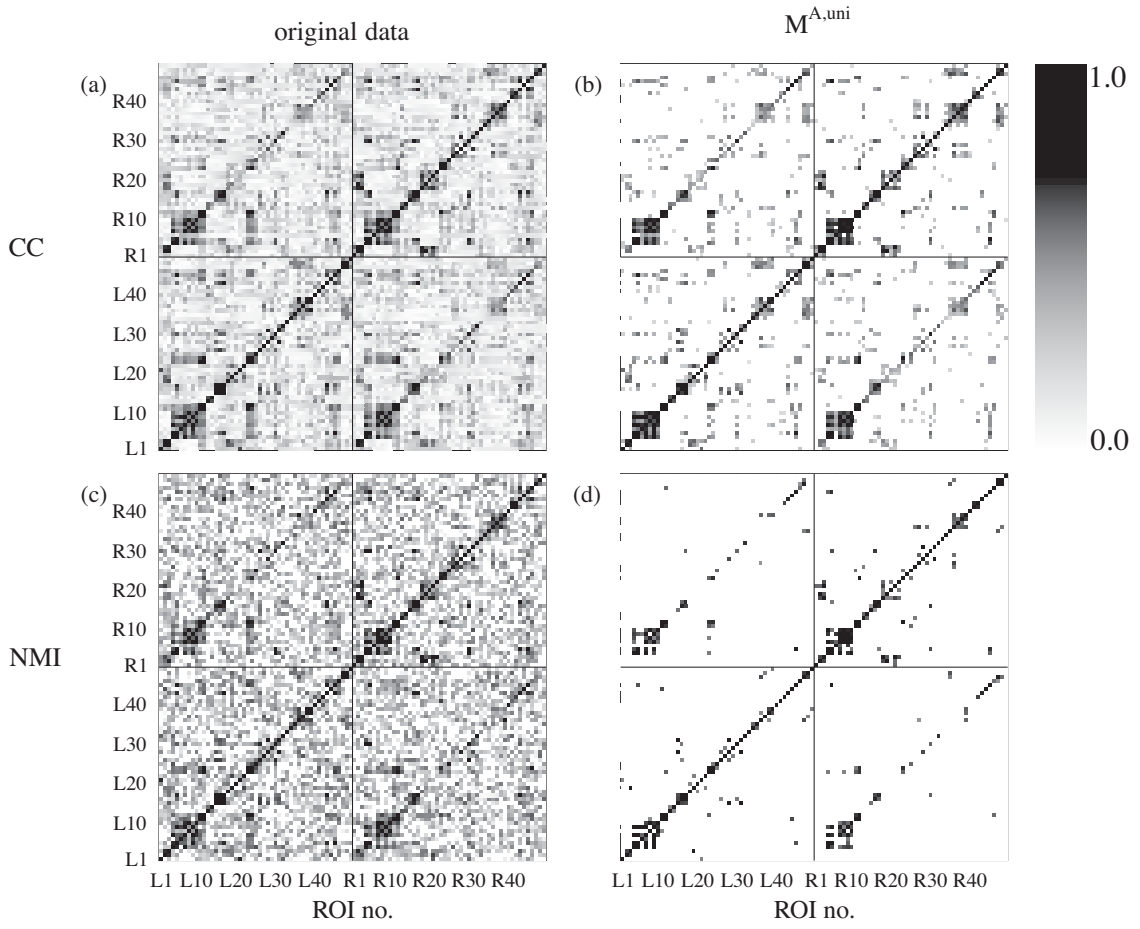

FIG. 5. Same as described in the caption to Fig. 4 but for subject 2.

and spaced at 2000 ms. A standard fMRI preprocessing protocol was implemented using the freely available MATLAB code for neuroimaging analysis (Statistical Parametric Mapping 5, SPM5, Wellcome Trust Centre for Neuroimaging, University College London, http://www.fil.ion.ucl.ac.uk/spm/software/spm5); see Ref. [30] for a brief general introduction. From the preprocessed data, time series (length 300 sample points) were extracted in three-dimensional ROIs from the Jülich histological atlas (JHA) [31]. The mean time courses of 49 gray-matter ROIs per hemisphere were used for further analysis.

All $M = 98$ ROI time series were regressed to the motion parameters (three orthogonal translations and three rotations) and the global signals of white matter and cerebrospinal fluid to minimize common influences. Finally, the residuals were bandpass filtered in the range $0.009\ \text{Hz} < f < 0.08\ \text{Hz}$ and subjected to interrelation analysis using the matrices $\mathcal{M}_{ij}^{A,B}$ defined in Eq. (7). For generation of $N_{\text{surr}} = 10$ surrogate time series $L = 256$ data points were used ignoring the first 30 time steps (60 s). Segments ($N_{\text{ens}} = 8$) of length $T = 120$ (4 min, overlap ~84%) were used to generate the ensembles.

In Figs. 4 and 5 we show a comparison of the interrelation matrices $\mathcal{M}_{ij}^{A,\text{uni}}$ [Figs. 4(b) and 5(b) and 4(d) and 5(d)] with the matrices C_{ij} [Figs. 4(a) and 5(a)] and NMI_{ij} [Figs. 4(c) and 5(c)] for both subjects. The normalization to independent univariate IAAFT surrogates eliminates the background and reveals the underlying pronounced interrelation pattern. For $\mathcal{M}_{ij}^{\text{CC,uni}}$ and model data this feature has been shown already in Ref. [16]. In the figures only absolute values of the matrix elements are shown. We note that only very few anticorrelated matrix elements turn out to be significant in the case of CC. The most prominent patterns of the normalized matrices are similar, regardless of the fact that only $\mathcal{M}_{ij}^{\text{NMI,uni}}$ is sensitive to both linear and nonlinear interrelation. The matrices NMI_{ij} have, in general, rather large positive values, which may confound multivariate analysis of the eigenvalues and eigenvectors by a huge repulsion between the largest and smaller eigenvalues and quasiuniform distribution of the components of the largest eigenvector. Similar to C_{ij} and $\mathcal{M}_{ij}^{\text{CC,uni}}$ the matrix $\mathcal{M}_{ij}^{\text{NMI,uni}}$ does not suffer from this problem.

The matrices $\mathcal{M}_{ij}^{A,\text{uni}}$ reveal a striking symmetry between the left (ROIs L1–L49) and right (ROIs R1–R49) hemisphere as can be seen from the repetition of diagonal blocks and clearly visible off-diagionals. Also remarkable is the similarity of interrelation matrix patterns across subjects. The strongly interrelated ROIs with number L4–L10 and R4–R10 correspond to a cluster representing the sensorimotor areas. Other examples for strongly interrelated clusters are ROIs L15–L17 and R15–R17, which represent main memory

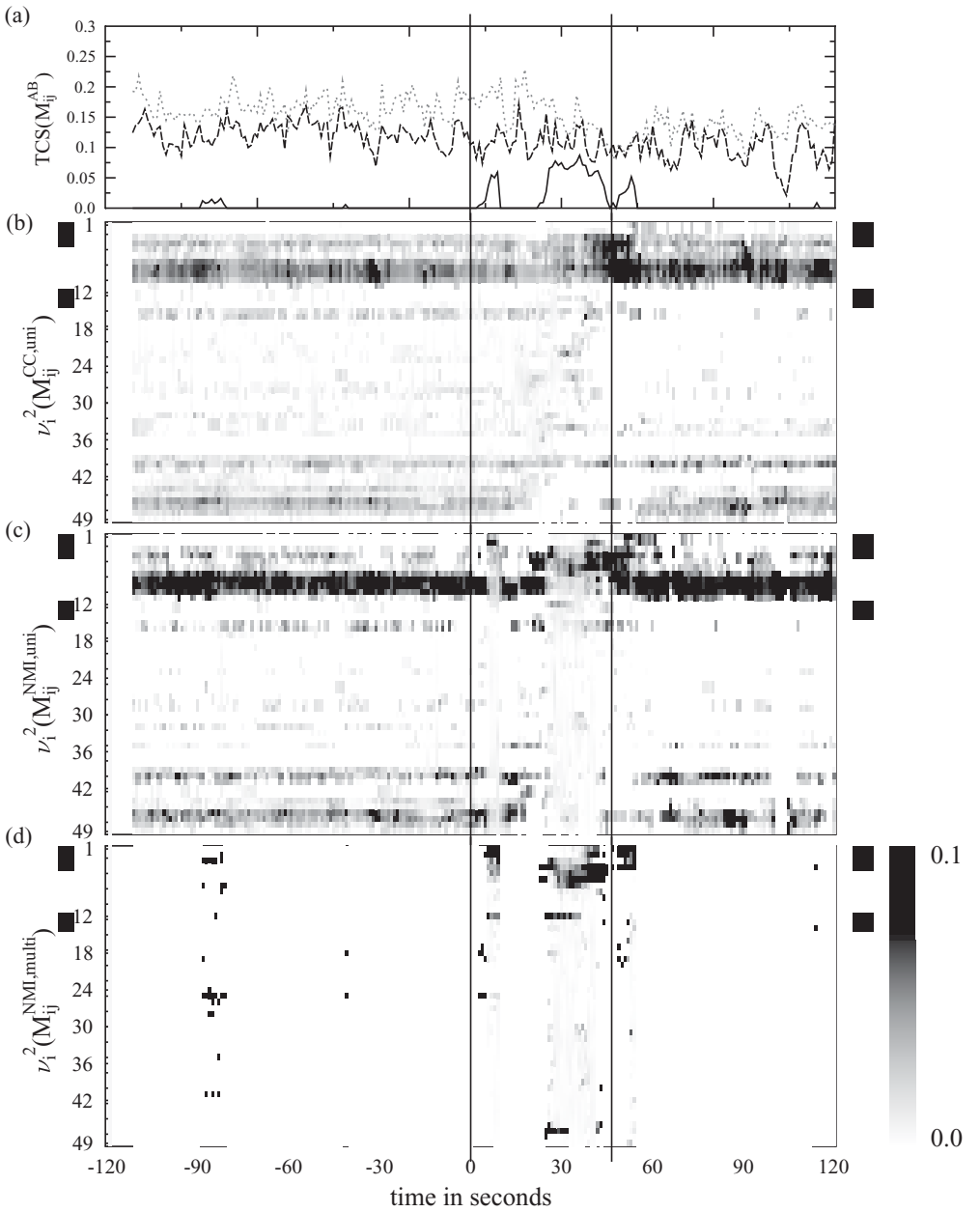

FIG. 6. Multivariate analysis of the interrelation patterns of a periseizure iEEG recording of patient 1 suffering from epileptic focal onset seizures. (a) TCS calculated from the matrices $\mathcal{M}_{ij}^{\mathrm{CC,uni}}$ (dotted in gray), $\mathcal{M}_{ij}^{\mathrm{NMI,uni}}$ (dashed in black), and $\mathcal{M}_{ij}^{\mathrm{NMI,multi}}$ (fully drawn in black). (b) Weighted sum ν_i^2 calculated from eigenvectors of the matrix $\mathcal{M}_{ij}^{\mathrm{CC,uni}}$; (c) weighted sum ν_i^2 calculated from eigenvectors of the matrix $\mathcal{M}_{ij}^{\mathrm{NMI,uni}}$; (d) weighted sum ν_i^2 calculated from eigenvectors of the matrix $\mathcal{M}_{ij}^{\mathrm{NMI,multi}}$. Electrographic seizure onset and termination are marked by vertical lines. The patient became seizure free after surgical removal of the brain tissue marked by black bars on the left and right of panels (b) to (d).

structures, and ROIs L11–L13 and R11–R13 (primary visual areas).

The matrices of Eq. (7) based on multivariate IAAFT surrogates are not shown in Figs. 4 and 5. As expected $\mathcal{M}_{ij}^{\mathrm{CC,multi}}$ turn out as identity matrices in both subjects. More surprisingly, also in the matrices $\mathcal{M}_{ij}^{\mathrm{NMI,multi}}$, not a single nonzero off-diagonal matrix element survives Bonferroni correction on significance level $\alpha = 0.01$ (i.e., $\alpha' = 2.1 \times 10^{-6}$), implying that the null hypothesis H_0^{multi} of entirely linear correlation cannot be rejected. Our observation is consistent with recent findings that nonlinear interrelation as measured by MI plays only a minor role in rsfMRI time series [14].

B. Periseizure intracranial electroencephalography

In addition to rsfMRI, we applied the matrices defined in Eq. (7) to a number of peri-seizure iEEG recordings of epilepsy patients, who were potential candidates for epilepsy surgery at the Inselspital Bern. To also demonstrate the potential usefulness of the matrices $\mathcal{M}_{ij}^{A,B}$ for these types of

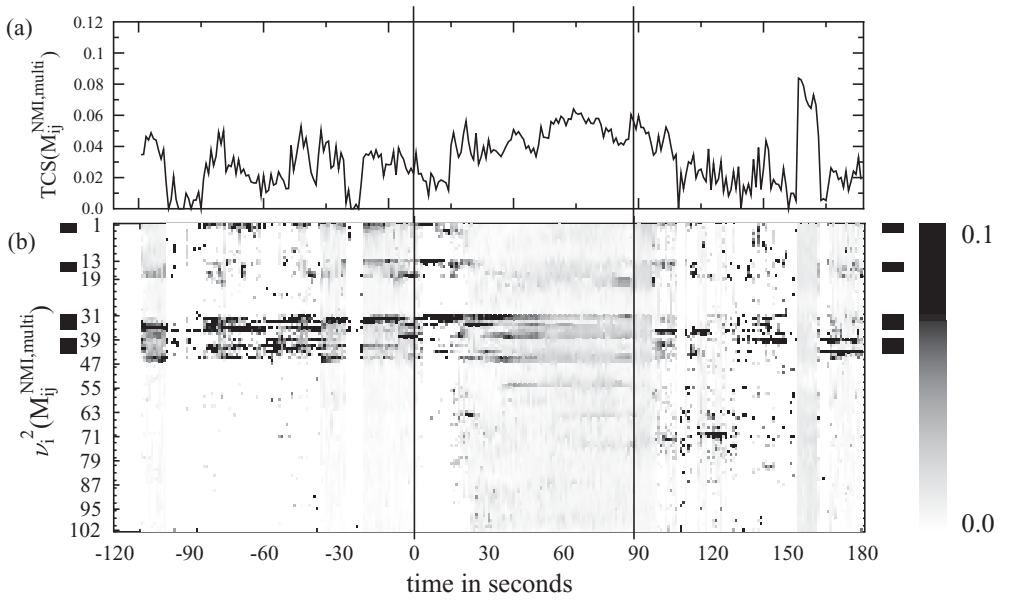

FIG. 7. Multivariate analysis of spatiotemporal patterns of the matrix $\mathcal{M}_{ij}^{\mathrm{NMI,multi}}$ for a periseizure iEEG recording of patient 2 suffering from epileptic focal onset seizures. (a) TCS; (b) weighted sum ν_i^2 calculated from the eigenvectors. Electrographic seizure onset and termination are marked by vertical lines. The patient became seizure free after surgical removal of the brain tissue marked by black bars on the left and right of panel (b).

data, we present two representative examples here. Patients suffered from long-standing pharmacoresistant epilepsy with focal-onset seizures and noninvasive studies had not allowed us to unequivocally localize the epileptogenic zone (defined as the brain region that is necessary and sufficient for seizure generation [32]). To decide on the possibility of epilepsy surgery, the patients had to undergo long-term iEEG with intracranial electrodes. They gave written informed consent that the long-term EEG data might be used for research purposes and our study was approved by the local ethics committee.

The iEEG was recorded at a sampling rate of 512 Hz using a NicoletOne recording system. For a detailed description of the amplifier specifications, see Ref. [33]. Before quantitative analysis the data were rereferenced to the median of all artifact-free channels and filtered in the range 0.5 to 150 Hz. The analyzed periseizure iEEG segments contained patient characteristic seizures and several minutes of pre- and postseizure recording. Seizure onset and termination times were visually defined by an experienced epileptologist/electroencephalographer (K.S.) and are indicated by vertical lines in Figs. 6 and 7. The iEEG recordings were analyzed using a moving window approach (steps of 1 s) with window length $L = 4096$ corresponding to 8 s such that four full cycles of the lowest frequency were contained. From these $N_{\mathrm{surr}} = 10$ univariate and multivariate IAAFT surrogate sets were sampled and for U tests ensembles of size $N_{\mathrm{ens}} = 10$ were generated shifting segments of length $T = 1024$ corresponding to 2 s within the larger windows (overlap $\sim$67%).

Figure 8 displays examples of the absolute interrelation matrices $\mathcal{M}_{ij}^{A,B}$ for a seizure of the first patient ($M = 49$ artifact-free iEEG channels, complex partial seizure of 46.5 s duration) taken at different time points relative to seizure onset. The matrix $\mathcal{M}_{ij}^{\mathrm{CC,uni}}$ (left column) shows genuine cross-correlation in blocks involving mainly the channels 3–5 and 7–10 (all located on a depth electrode implanted into the left temporal lobe) and 44–49 (left frontopolar strip electrode). As can be seen from Figs. 8(a), 8(d), and 8(g), the basic features of the linear correlation pattern are remarkably stable over time. Surgical removal of the tissue recorded by channels 1–4 and 12–14 led to seizure freedom in this patient. Consequently, the epileptogenic tissue must have been contained in the area these channels recorded from. Note that these channels apparently do not play a prominent role in the linear correlation patterns of Figs. 8(a), 8(d), and 8(g).

The matrix $\mathcal{M}_{ij}^{\mathrm{NMI,multi}}$ of interrelation that cannot be explained by the null hypothesis H_0^{multi} is shown in the right column. At seizure onset [Fig. 8(c)] it is the identity matrix, reflecting that nonlinear interrelation does not reach the level of significance at this time point in this patient. This situation is representative for pre- and postseizure situations; see Figs. 6(a) and 6(d). Eight seconds after seizure onset [Fig. 8(f)] there is pronounced nonlinear interrelation of channels 1 and 2 (the first two contacts on the tip of the depth electrode implanted into the left temporal lobe) and 12 (contact on the tip of the strip electrode covering the pole of the left temporal lobe) with each other and many other channels. Note that at the same time these channels are not involved in linear correlation patterns [Fig. 8(d)]. Later during seizure evolution ($t = 30$s, panel i) nonlinear interrelation is very pronounced for channels 3–7, 12, and 47. Remarkably, the linear and nonlinear interrelation *within* the surgically removed channels seems to be rather small at this stage [see Figs. 8(g) and 8(i)]. The middle column of Fig. 8 shows the matrix $\mathcal{M}_{ij}^{\mathrm{NMI,uni}}$ capturing

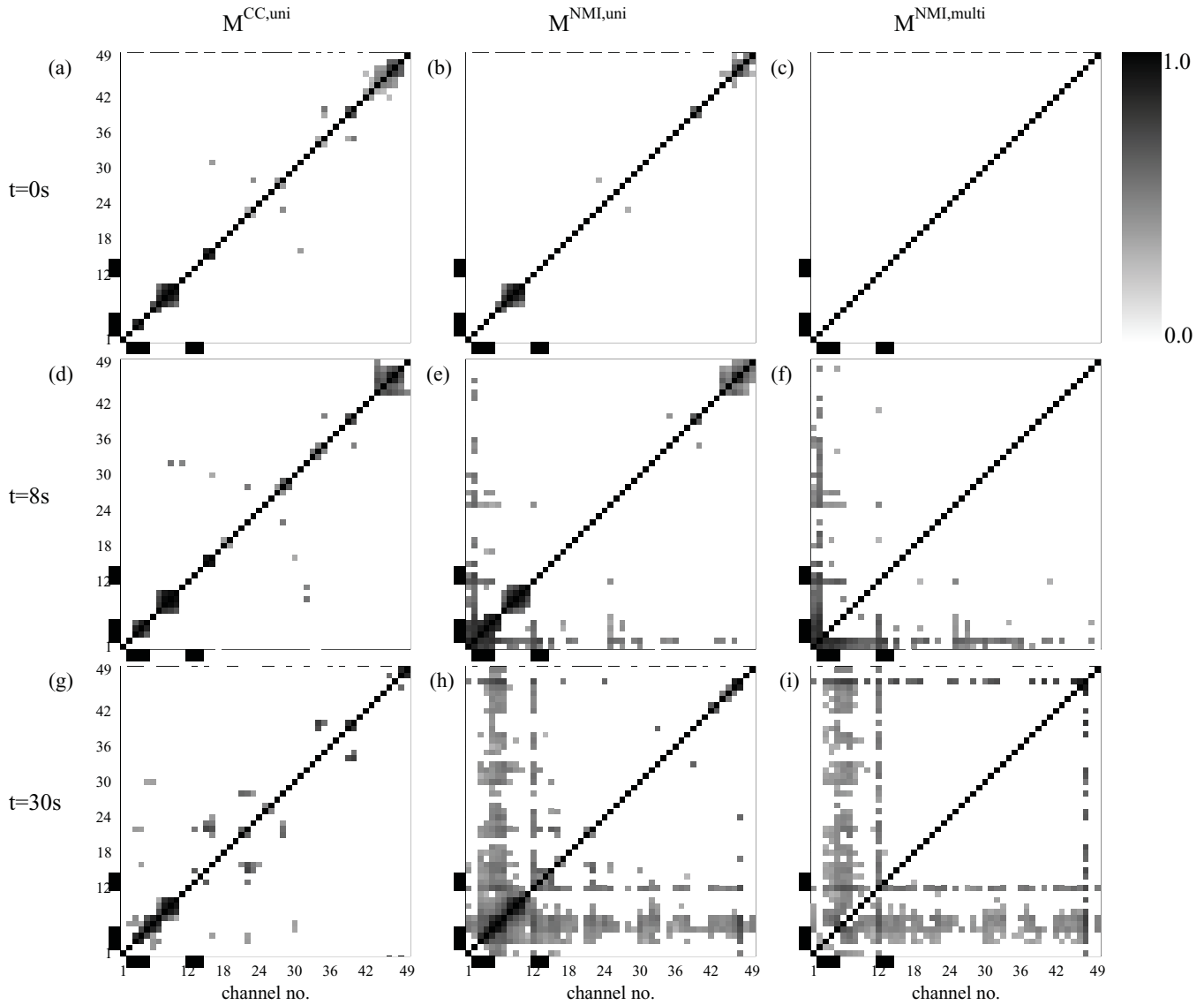

FIG. 8. Snapshots of absolute interrelation matrices $\mathcal{M}_{ij}^{A,B}$ for multivariate iEEG time series of an epilepsy patient taken at different times after seizure onset. The channels recording from tissue that was later surgically removed are indicated by black bars on the x and y axes.

linear as well as nonlinear interrelation. Essentially, it turns out to be a mixture of the matrices $\mathcal{M}_{ij}^{\mathrm{CC,uni}}$ and $\mathcal{M}_{ij}^{\mathrm{NMI,multi}}$.

To ease the interpretation of the matrix evolution in the course of time we employ rank-ordered eigenvalues $\lambda_l \geqslant \lambda_{l-1}$ and corresponding eigenvectors $\mathbf{v}_l$ of the matrices $\mathcal{M}_{ij}^{A,B}$ in the sequel. As a compact representation of the total interrelation present in the system, we use the coefficient of total correlation strength (TCS) introduced in [20]:

$$\mathrm{TCS} = \frac{1}{2(M-1)} \sum_{l=1}^{M} |\lambda_l - 1|. \tag{14}$$

Presence of significant interrelation in the matrix $\mathcal{M}_{ij}^{A,B}$ leads to a repulsion of some eigenvalues λ_l from 1. TCS normalizes the sum of these deviations in an appropriate way, yielding $\mathrm{TCS} = 0$ for fully independent and $\mathrm{TCS} = 1$ for identical time series. To represent the involvement of data channels in interrelation patterns in a compact way we calculate the following weighted sum of squared eigenvector components v_{il}^2:

$$\nu_i^2 = \frac{1}{2(M-1)\mathrm{TCS}} \sum_{l=1}^{M} |\lambda_l - 1|\, v_{il}^2. \tag{15}$$

The weighting factor $|\lambda_l - 1|$ assures that eigenvectors corresponding to repelled eigenvalues contribute with larger weight. Due to the larger absolute repulsion eigenvalues located at the upper end of the eigenvalue spectrum typically contribute stronger than those at the lower end. Eigenvectors that are not involved in any interrelation pattern are suppressed. Note that there is a certain similarity between Eq. (15) and the "participation indices" introduced in Refs. [34,35], which weight squared eigenvector components v_{il}^2 with the eigenvalues λ_l instead of the repulsion. The advantage of our definition is that also the eigenvalues located at the lower end of the spectrum contribute.

In Fig. 6(a) we show the temporal evolution of TCS calculated from the matrices $\mathcal{M}_{ij}^{A,B}$ of the first patient. TCS($\mathcal{M}_{ij}^{\mathrm{CC,uni}}$) and TCS($\mathcal{M}_{ij}^{\mathrm{NMI,uni}}$) behave very similarly. In pre- and postseizure phases TCS($\mathcal{M}_{ij}^{\mathrm{NMI,multi}}$) is basically zero. At the beginning and in the second half of the seizure this quantity is positive, implying that for this patient iEEG nonlinearities might be significant mainly during seizures. Using the model of Eqs. (8)–(13) we have checked that the performance of the matrices $\mathcal{M}_{ij}^{A,B}$ is independent of the spectral composition of time series for the chosen parameters (rsfMRI data or interictal or ictal iEEG data; data not shown). Therefore, we exclude artifacts of our surrogate implementation as a valid explanation for this observation.

The channels contributing to genuine cross-correlation patterns as measured by the eigenvectors of the matrix $\mathcal{M}_{ij}^{\mathrm{CC,uni}}$ are widely distributed and very stable temporally; see Fig. 6(b). The surgically removed tissue does not contribute to these patterns. Very similar observations can be made for the eigenvectors of $\mathcal{M}_{ij}^{\mathrm{NMI,uni}}$ [Fig. 6(c)]. This is true, although the matrix $\mathcal{M}_{ij}^{\mathrm{NMI,uni}}$ is a mixture of the matrices $\mathcal{M}_{ij}^{\mathrm{CC,uni}}$ and $\mathcal{M}_{ij}^{\mathrm{NMI,multi}}$ and consequently sensitive to linear and nonlinear interrelations alike (see Fig. 8).

In contrast, patterns measured by the matrix $\mathcal{M}_{ij}^{\mathrm{NMI,multi}}$ [Fig. 6(d)] display a pronounced temporal variation, which can easily be overlooked when analyzing multivariate quantities of inclusive interrelation measures like $\mathcal{M}_{ij}^{\mathrm{NMI,uni}}$ [Fig. 6(c)]. Around $t = 8$ s channels 1 and 2 contribute most to v_i^2; cf. Fig. 8(f). From $t = 20$s until seizure termination the nonlinear interrelation pattern differs, comprising mainly channels 3–7, 12, and 47; cf. Fig. 8(i). The pattern arising after seizure termination is similar to the example at $t = 8$ s.

Finally, we show the example of a periseizure iEEG recording of another patient ($M = 102$ artifact-free channels, complex partial seizure of 88 s duration) in Fig. 7. In contrast to the previous case, here the null hypothesis H_0^{multi} is rejected also before and after seizure, leading to a positive TCS [Fig. 7(a)]. Figure 7(b) reveals that the brain areas that mainly contribute to the eigenvectors are identical to the tissue whose surgical removal led to seizure freedom. The examples presented in Figs. 6 to 8 suggest that the matrices $\mathcal{M}_{ij}^{A,B}$ are a valuable tool for investigating linear and nonlinear aspects of the spatiotemporal iEEG dynamics of epileptic seizures. Comprehensive results will be published elsewhere.

V. SUMMARY AND DISCUSSION

In the present paper we generalized previously defined matrices [16] to Eq. (7), which offers a uniform approach to linear and nonlinear interrelations between time series. The matrix $\mathcal{M}_{ij}^{\mathrm{CC,uni}}$ is based on equal-time cross-correlation and employs independent univariate IAAFT surrogates for testing the null hypothesis of uncorrelated time series. It has nonzero elements only if for given data T the linear cross-correlation between the data is significantly larger than for fully independent surrogate time series with equal power spectrum. In contrast, the matrix $\mathcal{M}_{ij}^{\mathrm{NMI,multi}}$ is based on normalized mutual information and uses multivariate IAAFT surrogates as a reference. Consequently, nonzero elements indicate interrelations that are measurable by normalized MI but cannot be explained by surrogate data with conserved CC pattern. It is important that in this context "significantly nonlinear" interrelation is a stronger statement than significant interrelation as detected by a nonlinear measure.

The performance of the proposed framework was tested using a simple model allowing separate tuning of coupling (parameter $-1 \leqslant \rho \leqslant 1$) and nonlinearity (parameter $0 \leqslant \sigma \leqslant 1$); see Eqs. (8)–(13). The complementary character of $\mathcal{M}_{ij}^{\mathrm{CC,uni}}$ and $\mathcal{M}_{ij}^{\mathrm{NMI,multi}}$ and the inclusive character of $\mathcal{M}_{ij}^{\mathrm{NMI,uni}}$ was confirmed by these tests; see Fig. 2.

A special aspect of the definition Eq. (7) is the denominator, which independently puts all matrix elements on the same scale between 0 and ± 1. This is especially important for $\mathcal{M}_{ij}^{\mathrm{NMI,multi}}$ where deviations between original and surrogate data are often highly significant but small in absolute size. Without the normalizing denominator such effects could easily remain undetected, especially when aiming at multivariate analysis in terms of matrix eigenvalues and eigenvectors.

The employment of U tests for significance checking [factor $s_{ij} \in \{0,1\}$ in Eq. (7)] may seem artificial at first sight as it requires two segment lengths (L and $T < L$) as well as generation of ensembles of size N_{ens} (whose members should be as independent as possible) to calculate the medians μ_{ij} and ν_{ij} of the interrelation measure A_{ij}. A more intuitive approach to the significance s_{ij} consists in sampling $m/\alpha' - 1$ surrogates ($L = T$, $N_{\mathrm{ens}} = 1$ and m is an oversampling factor) and rejecting the null hypothesis on significance level $\alpha' = 2\alpha/(M-1)/M$ if $|A_{ij}|$ is larger than the mth largest value found for the surrogates. To exclude sensitivity to outliers in the sample the data should be oversampled by a factor $m \gg 1$, a strategy which has been followed in Ref. [14] ($\alpha = 0.05$, $m = 5$, $M = 2$, *no* Bonferroni correction). We have checked that this approach is computationally feasible for the bivariate case and produces results very similar to those shown in Figs. 1 and 2.

For large $M \gg 2$ and $m \gg 1$, however, the extensive surrogate generation becomes computationally prohibitive, whereas in our approach the workload is limited to N_{surr} IAAFT surrogates. As except for extremely small N_{surr} the results are almost independent, this parameter can be chosen to be rather small; see Figs. 1(b) and 1(d). Similarly, we have checked the dependence of our results on the overlap of the segments of size T as determined by the parameter N_{ens}. For not-too-large overlaps we found only small variations; see Figs. 1(a) and 1(c).

Application of the matrices $\mathcal{M}_{ij}^{A,B}$ in situations without temporal evolution is easily feasible. Using $N_{\mathrm{surr}} = 10$, the calculation of the matrices shown in Figs. 4 and 5 took approximately 10 min on a desktop computer with 2.0-GHz CPU. In contrast, a time-dependent application as shown in Figs. 6 and 7 remains computationally demanding due to repeated generation of univariate and multivariate IAAFT surrogate ensembles of size N_{surr} on every time step. For example, the same computer calculated for more than 2 days to produce the matrices underlying Fig. 6 with a time resolution of 1 s.

Further generalization of the matrices $\mathcal{M}_{ij}^{A,B}$ defined in Eq. (7) to other bivariate interrelation measures A is possible.

The merit of using partial correlation matrices [36,37] and partial mutual information matrices [38] is currently under investigation. Moreover, generalization to different types of surrogates B is conceivable. To reduce computation time in our application the iterative amplitude adjustment could be dropped from the procedure as also done in Refs. [12,14]. If L is large enough to contain many cycles of the slowest frequency present in the data and only H_0^{uni} were to be tested without testing H_0^{multi} as well, the much faster shift surrogates could be considered [39]. Other examples include pseudoperiodic surrogates [40], which are especially suitable for systems with strong periodicities, or twin surrogates [41,42], which allow testing the null hypothesis of absence of phase synchronization.

For compact representation of all eigenvectors of the matrices $\mathcal{M}_{ij}^{A,B}$ we introduced in Eq. (15) the weighted sum of squared components. This measure summarizes which data channels contribute prominently to any of the eigenvectors (see Figs. 6 and 7) and large eigenvalue repulsion at both ends of the eigenvalue spectrum is weighted as stronger.

Although the proposed framework is not limited to neurophysiological data, we have shown two examples of possible application. In resting-state fMRI data multivariate correlation analysis on basis of the matrix $\mathcal{M}_{ij}^{\text{CC,uni}}$ revealed linear resting-state functional connectivity patterns among predefined homologous cytoarchitectonic ROIs known to sustain sensorimotor and visual functions that were reproducible between two subjects; see Figs. 4 and 5. In agreement with Ref. [14] where technical details of the implementation were treated differently (e.g., different ROI definition, use of noniterative procedures instead of IAAFT surrogates, and no Bonferroni correction for multiple testing), using MI we found that nonlinear interrelation is of minor importance in resting-state data.

As a second example the matrices of Eq. (7) were applied to representative intracranial EEG recordings of two epilepsy patients. We found that during seizure linear and nonlinear interrelation can be complementary to each other. Although in relatively long pre- and postseizure parts of the recording the interrelation pattern of nonepileptogenic brain areas is well described by linear cross-correlation, it might miss important nonlinear interrelation of epileptogenic tissue and during seizure (Figs. 6 to 8). Note that nonlinear measures alone, i.e., without testing the null hypothesis of linear correlation, could also miss these effects.

Our result that interictal EEG can well be described by linear properties with nonlinearities mainly confined to epileptic seizures and seizure generating tissue is in line with previous findings. For *univariate* EEG properties of healthy subjects it was shown that only very small parts of the respective EEG data sets were *not* compatible with linear dynamics, with examples including the correlation dimension [5,43] and the nonlinear prediction error [44]. For epilepsy patients it was found in Ref. [45] using the correlation integral that nonlinearities of iEEG signals recorded from epileptogenic brain regions were more significant than those recorded from healthy regions. In Refs. [43,46] a significantly lowered correlation dimension of ictal EEG signals was found. Intracranial EEG showed its confinement mainly within and near the seizure onset zone. Analyzing different types of EEG recorded from epilepsy patients and using the nonlinear prediction error as well as effective correlation dimension [47], it was found that nonlinearities are strongest during epileptic seizures and for seizure generating tissue.

In Ref. [48] nonseizure iEEG of 29 patients suffering from mesial temporal lobe epilepsy was analyzed using several linear and nonlinear univariate measures. Lateralization of the epileptic focus was best when nonlinear measures were corrected for IAAFT surrogates. Very recently, these authors conducted a similar study using linear and nonlinear bivariate measures, finding increased interrelation in the focal hemisphere [15]. Moreover, significance and accuracy of focus lateralization turned out highest if a nonlinear interrelation measure based on rank statistics [49] was corrected for bivariate IAAFT surrogates. Although the applied nonlinear interrelation measure differs, our bi- and multivariate results are consistent with these recent findings.

The relation between epileptogenic tissue and iEEG channels rejecting the null hypothesis H_0^{multi} before or during seizure seems interesting but nontrivial and is the topic of ongoing research. Combined application of the matrices $\mathcal{M}_{ij}^{\text{CC,uni}}$ and $\mathcal{M}_{ij}^{\text{NMI,multi}}$ to larger clinical cohorts of rsfMRI and iEEG data sets is underway and will be published elsewhere.

ACKNOWLEDGMENTS

This work was supported by Deutsche Forschungsgemeinschaft, Germany (Grant No. RU 1401/2-1), Schweizerischer Nationalfonds, Switzerland (project nos. 320030-122010, 3200B0-1108018, and 33CM30-124089) and CONACyT, Mexico (project no. 48500). The authors thank the anonymous reviewers for their constructive remarks.

[1] H. Kantz and T. Schreiber, *Nonlinear Time Series Analysis*, 2nd ed. (Cambridge University Press, Cambridge, 2004).

[2] C. Stam, Clin. Neurophysiol. **116**, 2266 (2005).

[3] E. Pereda, R. Quian Quiroga, and J. Bhattacharya, Prog. Neurobiol. **77**, 1 (2005).

[4] P. E. Rapp, T. R. Bashore, J. M. Martinerie, A. M. Albano, and A. I. Mees, Brain Topogr. **2**, 99 (1989).

[5] J. Theiler and P. E. Rapp, Electroencephalogr. Clin. Neurophysiol. **98**, 213 (1996).

[6] K. Ansari-Asl, L. Senhadji, J.-J. Bellanger, and F. Wendling, Phys. Rev. E **74**, 031916 (2006).

[7] T. Kreuz, F. Mormann, R. G. Andrzejak, A. Kraskov, K. Lehnertz, and P. Grassberger, Physica D **225**, 29 (2007).

[8] F. Wendling, K. Ansari-Asl, F. Bartolomei, and L. Senhadji, J. Neurosci. Methods **183**, 9 (2009).

[9] F. Mormann, T. Kreuz, C. Rieke, R. G. Andrzejak, A. Kraskov, P. David, C. E. Elger, and K. Lehnertz, Clin. Neurophys. **116**, 569 (2005).

[10] F. Mormann, R. G. Andrzejak, C. E. Elger, and K. Lehnertz, Brain **130**, 314 (2007).
[11] R. G. Andrzejak, A. Kraskov, H. Stögbauer, F. Mormann, and T. Kreuz, Phys. Rev. E **68**, 066202 (2003).
[12] M. A. Kramer, U. T. Eden, S. S. Cash, and E. D. Kolaczyk, Phys. Rev. E **79**, 061916 (2009).
[13] I. Vlachos and D. Kugiumtzis, Phys. Rev. E **82**, 016207 (2010).
[14] J. Hlinka, M. Palus, M. Vejmelka, D. Mantini, and M. Corbetta, NeuroImage **54**, 2218 (2010).
[15] R. Andrzejak, D. Chicharro, K. Lehnertz, and F. Mormann, Phys. Rev. E **83**, 046203 (2011).
[16] C. Rummel, M. Müller, G. Baier, F. Amor, and K. Schindler, J. Neurosci. Methods **191**, 94 (2010).
[17] H. Joe, J. Am. Stat. Assoc. **84**, 157 (1989).
[18] A. Kraskov, H. Stögbauer, and P. Grassberger, Phys. Rev. E **69**, 066138 (2004).
[19] S. Khan, S. Bandyopadhyay, A. R. Ganguly, S. Saigal, D. J. Erickson III, V. Protopopescu, and G. Ostrouchov, Phys. Rev. E **76**, 026209 (2007).
[20] M. Müller, G. Baier, C. Rummel, and K. Schindler, Europhys. Lett. **84**, 10009 (2008).
[21] T. Schreiber and A. Schmitz, Phys. Rev. Lett. **77**, 635 (1996).
[22] T. Schreiber and A. Schmitz, Physica D **142**, 346 (2000).
[23] S. Siegel, *Non-parametric Statistics for the Behavioral Sciences* (McGraw-Hill, New York, 1956).
[24] C. Rummel, M. Müller, and K. Schindler, Phys. Rev. E **78**, 066703 (2008).
[25] K. Friston, Hum. Brain Mapp. **2**, 56 (1994).
[26] M. D. Fox and M. Raichle, Nat. Rev. Neurosci. **8**, 700 (2007).
[27] B. Biswal, F. Z. Yetkin, V. M. Haughton, and J. S. Hyde, Magn. Reson. Med. **34**, 537 (1995).
[28] J. S. Damoiseaux, S. A. Rombouts, F. Barkhof, P. Scheltens, C. J. Stam, S. M. Smith, and C. F. Beckmann, Proc. Natl. Acad. Sci. U.S.A. **103**, 13848 (2006).
[29] M. D. Greicius, B. Krasnow, A. L. Reiss, and V. Menon, Proc. Natl. Acad. Sci. U.S.A. **100**, 253 (2003).
[30] N. F. Ramsey, H. Hoogduin, and J. M. Jansma, Eur. Neuropsychopharmacol. **12**, 517 (2002).
[31] K. Amunts and K. Zilles, Neuroimag. Clin. N. Am. **11**, 151 (2001).
[32] F. Rosenow and H. Lüders, Brain **124**, 1683 (2001).
[33] K. Schindler, F. Amor, H. Gast, M. Müller, A. Stibal, L. Mariani, and C. Rummel, Epilepsy Res. **89**, 72 (2010).
[34] C. Allefeld, M. Müller, and J. Kurths, Int. J. Bifurcat. Chaos **17**, 3493 (2007).
[35] S. Bialonski and K. Lehnertz, Phys. Rev. E **74**, 051909 (2006).
[36] T. Anderson, *An Introduction to Multivariate Statistical Analysis* (Wiley, New York, 2003).
[37] D. F. Morrison, *Multivariate Statistical Methods*, 4th ed. (Thomson, Belmont, 2005).
[38] S. Frenzel and B. Pompe, Phys. Rev. Lett. **99**, 204101 (2007).
[39] T. I. Netoff and S. J. Schiff, J. Neurosci. **22**, 7297 (2002).
[40] M. Small, D. Yu, and R. G. Harrison, Phys. Rev. Lett. **87**, 188101 (2001).
[41] M. Thiel, M. C. Romano, J. Kurths, M. Rolfs, and R. Kliegl, Europhys. Lett. **75**, 535 (2006).
[42] M. C. Romano, M. Thiel, J. Kurths, K. Mergenthaler, and R. Engbert, Chaos **19**, 015108 (2009).
[43] H. Jing and M. Takigawa, Biol. Cybern. **83**, 391 (2000).
[44] R. A. Stepien, Acta Neurobiol. Exp. **62**, 277 (2002).
[45] M. C. Casdagli, L. D. Iasemidis, R. S. Savit, R. L. Gilmore, S. N. Roper, and J. C. Sackellares, Electroencephalogr. Clin. Neurophysiol. **102**, 98 (1997).
[46] J. P. M. Pijn, D. N. Velis, M. J. van der Heyden, J. DeGoede, C. W. van Veelen, and F. H. Lopes da Silva, Brain Topogr. **9**, 249 (1997).
[47] R. G. Andrzejak, K. Lehnertz, F. Mormann, C. Rieke, P. David, and C. E. Elger, Phys. Rev. E **64**, 061907 (2001).
[48] R. Andrzejak, F. Mormann, G. Widman, T. Kreuz, C. Elger, and K. Lehnertz, Epilepsy Res. **69**, 30 (2006).
[49] D. Chicharro and R. G. Andrzejak, Phys. Rev. E **80**, 026217 (2009).